

Engineered Fibrillar Fibronectin Networks as Three-Dimensional Tissue Scaffolds

Stacy Jordahl, Luis Solorio, Dylan B. Neale, Sean McDermott, Jacob H. Jordahl, Alexandra Fox, Christopher Dunlay, Annie Xiao, Martha Brown, Max Wicha, Gary D. Luker, and Joerg Lahann*

Extracellular matrix (ECM) proteins, and most prominently, fibronectin (Fn), are routinely used in the form of adsorbed pre-coatings in an attempt to create a cell-supporting environment in both two- and three-dimensional cell culture systems. However, these protein coatings are typically deposited in a form which is structurally and functionally distinct from the ECM-constituting fibrillar protein networks naturally deposited by cells. Here, the cell-free and scalable synthesis of freely suspended and mechanically robust three-dimensional (3D) networks of fibrillar fibronectin (fFn) supported by tessellated polymer scaffolds is reported. Hydrodynamically induced Fn fibrillogenesis at the three-phase contact line between air, an Fn solution, and a tessellated scaffold microstructure yields extended protein networks. Importantly, engineered fFn networks promote cell invasion and proliferation, enable in vitro expansion of primary cancer cells, and induce an epithelial-to-mesenchymal transition in cancer cells. Engineered fFn networks support the formation of multicellular cancer structures cells from plural effusions of cancer patients. With further work, engineered fFn networks can have a transformative impact on fundamental cell studies, precision medicine, pharmaceutical testing, and pre-clinical diagnostics.

The extracellular matrix (ECM) constitutes the proteinaceous microenvironment of all multicellular tissues^[1] and serves as a model for three-dimensional (3D) in vitro cell culture design.^[2] Changes in ECM structure and composition drive biological function in both healthy and diseased states.^[3] Fibronectin (Fn) is one of the most abundant ECM proteins in normal tissues,^[4]

and increased Fn expression is associated with multiple cancers.^[5] During breast cancer progression, fibrillar Fn (fFn) promotes tumorigenesis and metastasis, partly due to an epithelial-to-mesenchymal transition (EMT) in malignant cells.^[6] Furthermore, upregulation of Fn has been identified to be a key step during pre-metastatic niche formation.^[7]


A mechanosensitive protein, Fn exists in a compact state when solubilized such as in blood plasma, and in various stretched states such as fFn when localized in ECM.^[4,8] The structure and conformation of Fn governs the exposure or sequestration of binding sites that impact its biological function and cell response.^[8b,9] Fn fibrillogenesis involves unfolding of the protein via mechanical translocation of integrins bound to cell surface receptors. Structurally, unfolding occurs largely at the mechanosensitive type III domain (Fn-3) exposing self-association sites for subsequent fibrillogenesis.^[4,8b,10] Despite years of study, a comprehensive understanding of each region of

the type I, II, and III Fn domains and how they interact with one another or cells to govern fibril formation is still a topic of ongoing research.^[11]

We discovered that hydrodynamically induced fibrillogenesis at the three-phase contact line between air, an Fn solution, and a tessellated porous scaffold yields remarkably stable fFn

Dr. S. Jordahl, Dr. L. Solorio, D. B. Neale, Dr. S. McDermott, Dr. J. H. Jordahl, A. Fox, C. Dunlay, Prof. M. Wicha
Biointerfaces Institute
University of Michigan
2800 Plymouth Road, Ann Arbor, MI 48109, USA
A. Xiao, Dr. G. D. Luker
Department of Radiology, Microbiology and Immunology, Biomedical Engineering
University of Michigan
109 Zina Pitcher Place, Ann Arbor, MI 48109, USA

M. Brown
Department of Internal Medicine
University of Michigan
1500 E Medical Center Dr SPC 5916, Ann Arbor, MI 48109, USA
Prof. J. Lahann
Biointerfaces Institute
Departments of Chemical Engineering, Materials Science and Engineering, Biomedical Engineering, and Macromolecular Science and Engineering
University of Michigan
2800 Plymouth Road, Ann Arbor, MI 48109, USA
E-mail: lahann@umich.edu

 The ORCID identification number(s) for the author(s) of this article can be found under <https://doi.org/10.1002/adma.201904580>.

DOI: 10.1002/adma.201904580

networks that promote cell invasion and proliferation, enable in vitro expansion of primary cancer cells, and induce EMT. These engineered fFn networks can serve as an engineering platform for the design of in vitro 3D culture systems, including tumor models which would impact fundamental studies of tumorigenesis and advance our ability to directly expand primary patient cancer cells.

The cell-free synthesis of scalable, mechanically robust 3D networks of fFn suspended across a scaffold support would constitute a critical technological advance in engineered biomaterials systems. Cell-free fibrillogenesis has been previously observed by simple shearing of Fn solution, drawing of individual fibers,^[12] extraction of fibrillar mats^[13] from Fn solutions, or through the use of mechanical,^[14] or interfacially active denaturants.^[4,14,15] However, these methods suffer from several limitations including manual positioning of protein fibers or networks,^[12,13] low throughput,^[12] or the need to chemically crosslink the protein to ensure fiber stabilization.^[13b] In

application to cell culture and cell analyses, these methods often lack: i) effective cell invasion and cell removal capabilities,^[13a] ii) transparency for microscopy techniques,^[4,12,13] iii) a support where cells can deposit their own matrix or remain adhered after degrading the original protein matrix,^[13a,16] and iv) sufficiently large areas ($\geq 0.2 \text{ mm}^2$) of 3D space free of synthetic material. When polymer scaffolds are used to mediate some of these shortcomings, the support material itself can act as a barrier for cell invasion and uninterrupted transport of nutrients.^[2,4,12,14,15] In contrast, we found that gentle shearing (angular velocity of 8 rpm) of an Fn solution at the three-phase contact line defined by the protein solution, air, and a support comprised of tessellated $500 \times 500 \mu\text{m}$ square pores yields insoluble networks of fFn, even in the absence of denaturants (**Figure 1**). Fn used in this study was commercially available, purified Fn isolated from blood plasma. The tessellated microfiber scaffolds were prepared from poly(lactide-co-glycolide) (PLGA) by 3D jet writing.^[17] While the scaffold size, pore geometries, and

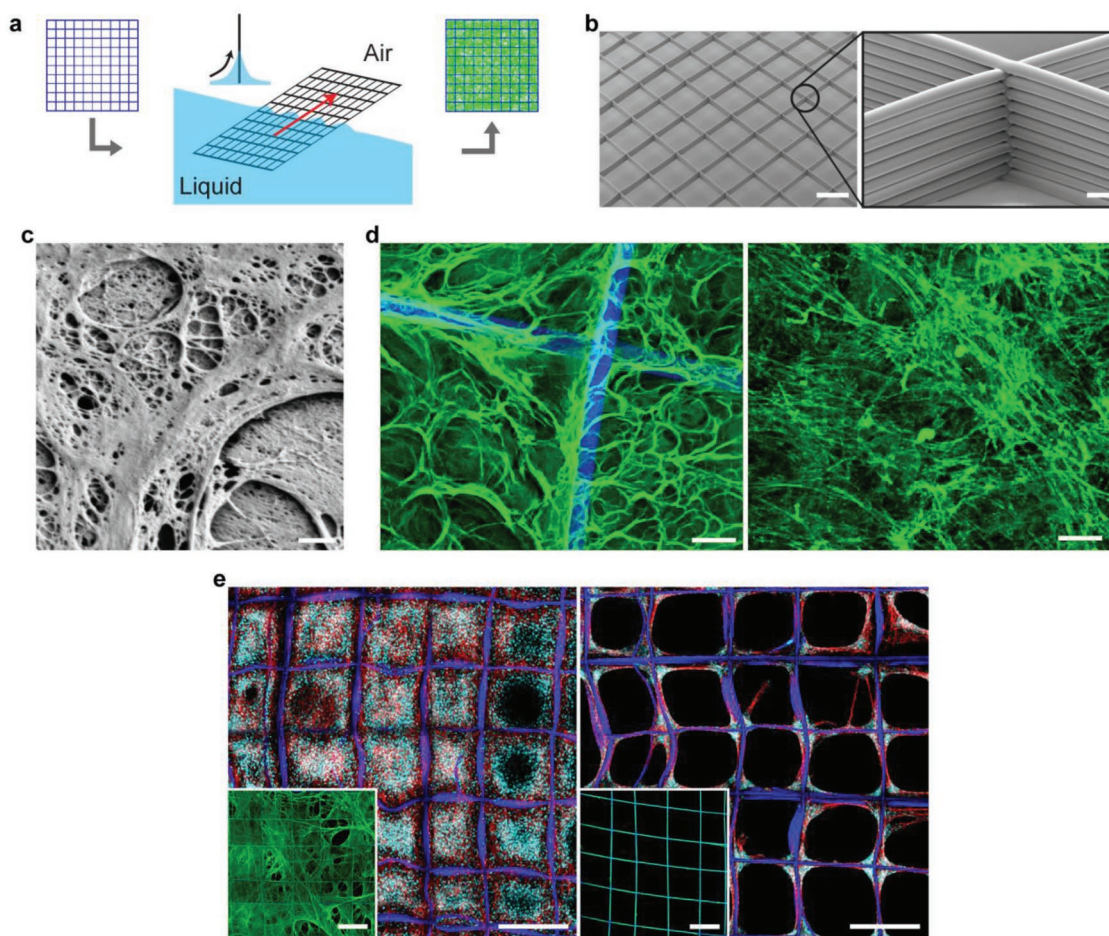


Figure 1. Hydrodynamically induced fibrillogenesis of Fn. a) Fluid shear is applied at the three-phase interface of a porous scaffold, air, and an Fn solution resulting in the deposition of a network of insoluble Fn fibrils (fFn) suspended across the scaffold, i.e., fFn networks. b) Polymer microfiber scaffolds fabricated via 3D jet writing featuring tessellated square pores. Scale bars $500 \mu\text{m}$ (left) and $25 \mu\text{m}$ (inset). c) High-resolution SEM of fFn freely suspended within a pore of the scaffold. Scale bar $1 \mu\text{m}$. d) Left) LSCM of fFn (green) suspended within the scaffold (blue) for comparison to right) Fn deposited by human mammary fibroblasts cultured on glass and subsequently decellularized. Scale bar $25 \mu\text{m}$. e) NIH-3T3 mouse fibroblasts cultured three days on either left) an fFn network or right) Fn statically adsorbed onto a scaffold. Insets show representative images of the morphology and distribution of Fn (green) deposited on scaffolds (blue) either by hydrodynamic shearing at the three-phase interface (left inset) or static adsorption (right inset). Channels: blue, tessellated scaffold; green, Fn; cyan, cell nucleus; and red, actin. Scale bars $500 \mu\text{m}$.

thickness are tunable, all scaffolds used in this study spanned an area of 34.8 mm² featuring square pores with a free volume of 96% and an overall thickness of 0.12 mm (Figure 1b). The thickness of the engineered fFn networks was chosen for optimal imaging results and to allow cells to perfuse in or out, while providing large volumes of freely suspended protein matrix for cell growth in three dimensions. The fFn networks were mechanically robust for easy handling during culture, and readily implemented by standard cell culture techniques in a multiwell plate.

Within 15 min, hydrodynamically induced fibrillogenesis resulted in emerging networks of insoluble Fn fibrils that extended across the entire scaffold at lengths approaching several millimeters (Figure 1c, and Figure S1b–d,f, Supporting Information). The absence of a shear force (Figure S1f, Supporting Information and insets of Figure 1e), or hydrodynamic shearing over a smooth, non-porous support (Figure S1a, Supporting Information) did not result in fibrillar networks. We instead observed a conformal Fn coating. The total amount of Fn loaded onto a single scaffold by hydrodynamically induced fibrillogenesis was 12-fold higher than the amount of protein detected for conformally coated scaffolds (Figure S1e, Supporting Information). The fFn networks displayed morphological similarities to matrix deposited by human fibroblasts (Figure 1d, and Figure S2a,b, Supporting Information).

Engineered fFn networks proved to be insoluble in a 1% deoxycholate solution (Figure S3, Supporting Information), another feature of biologically derived Fn matrix.^[18] Importantly, fFn networks supported confluent cell culture that extended throughout the entire scaffold volume (Figure 1e, and Figure S4, Supporting Information). In contrast, identical scaffolds that were conformally coated with Fn did not promote continuous cell coverage of the open pore areas (Figure 1e). A wide range of mammalian cell types including normal cells (fibroblast and endothelial cells), cancer cells (breast and pancreatic cancer cells), and mesenchymal stem cells^[17] formed confluent 3D cell cultures in as little as three days (Figure 1e, and Figures S4 and S5, Supporting Information).

Engineered fFn networks, but not conformally deposited Fn, stained positively with an Fn-3 antibody indicating exposed cellular Fn after hydrodynamic fibrillogenesis (Figures S6 and S2b, Supporting Information). This resembled the staining of Fn deposited by human mammary fibroblasts (Figure S2a, Supporting Information, stained after removal of the cells). In contrast, statically adsorbed Fn on either tessellated scaffolds or tissue culture polystyrene (TCPS) was not recognized by the Fn-3 antibody (Figure S2c,d, Supporting Information). For further validation, an IST-9 antibody was used since its specificity to the alternatively spliced domain A (EIIIA or EDA), a cellular Fn variant within the type III region of Fn, is well documented.^[19] When directly comparing engineered fFn networks to Fn statically deposited onto non-woven mats (a scaffold of randomly deposited PLGA fibers), we found that the Fn-3 and IST-9 antibodies only recognized the fFn networks and not the Fn conformally deposited onto non-woven mats (Figure S7, Supporting Information).^[19a] To definitively confirm the presence of EDA(+) Fn in our protein source, liquid chromatography mass spectrometry-based (LC-MS) proteomics was performed. As expected, the main constituent was Fn with 71–82% sequence coverage (Figure S8c, Supporting Information). Annotated

MS/MS spectra for tryptic EDA peptides GLAFTDQVDSIK and IAWESPQGVSR are shown in Figure S8a,b in the Supporting Information. The EDA fragments are expected to be identified after trypsin digestion and indeed were identified with nearly complete sequencing, confirming the presence of EDA(+) Fn in our protein source. Although, plasma Fn isoforms are the main constituent of Fn in blood plasma, previous studies have reported that small fractions of cellular Fn can circulate in the blood of healthy patients.^[20]

Collectively, these data suggest that EDA(+) Fn within our protein source is physically exposed only after hydrodynamic fibrillogenesis, and is not available for antibody binding when Fn is conformally adsorbed onto a surface. We note that the role of the EDA peptide in Fn biology is a topic of ongoing research. While this variant is not believed to be a requisite for fibrillogenesis,^[21] some studies have shown it plays an important role by leading to more robust fibrillar networks secreted by cells.^[22] Additionally, while some report recombinant EDA(+) Fn coated onto a surface may enhance cell migration,^[23] other studies have suggested that knockdown of EDA-Fn secretion impedes cell motility even on Fn-coated substrates.^[24] Missirlis et al. discuss potentially conflicting results researchers have reported with respect to the role of EDA-Fn in cell motility.^[24] Finally, the mechanosensitivity of the EDA domain is not well known^[25] and warrants further investigation. Hence, it is reasonable that changes in Fn binding activity may occur when Fn is presented in a fibrillar state compared to a conformal surface coating, which has not yet been directly investigated. These many unknowns underscore the need for a native-like fFn cell culture platform. We thus concluded that our Fn fibril production and characterization results are consistent with a mechanism where interfacial shearing induces mechanical deformation of solute Fn that extends the protein, enabling self-polymerization, and fiber formation. This is analogous to the mechanically induced unfolding of the Fn molecule during cell-driven,^[9b,26] as well as previously reported shear-driven fibrillogenesis.^[4,8a,27] In contrast to the widely used conformal Fn pre-coatings, hydrodynamically induced fibrillogenesis not only results in a stable, fibrillar matrix readily applicable to 3D cell culture, but also provides access to ECM mimics with biologically distinct properties.^[10a,28]

Recognizing the prominence of Fn in primary breast cancer ECM,^[29] we tested the ability of fFn networks to enhance tumor engraftment of breast cancer cells in a murine model of epithelial breast cancer. We cultured AT-3 murine breast cancer cells that stably expressed firefly luciferase^[30] onto fFn networks. After three days, cells had infiltrated the entire scaffold (Figure 2a,b, and Figure S9a,b, Supporting Information), while still remaining in a proliferative state (Figure S9c, Supporting Information).

The fFn networks carrying 30 000 cells per scaffold were orthotopically implanted into immunocompetent C57BL/6 mice. Bioluminescence imaging revealed initial signs of tumorigenesis as early as two days after implantation (Figure S10, Supporting Information). For comparison, the cell suspension of an equivalent number of AT-3 cells did not support tumor engraftment over 21 d (Figure 2c, and Figure S10, Supporting Information). Histology of engrafted tumors confirmed natural invasion of cancer cells from the fFn networks into adjacent tissue (Figure 2d). Pre-seeded with 30 000 AT-3 cells, fFn

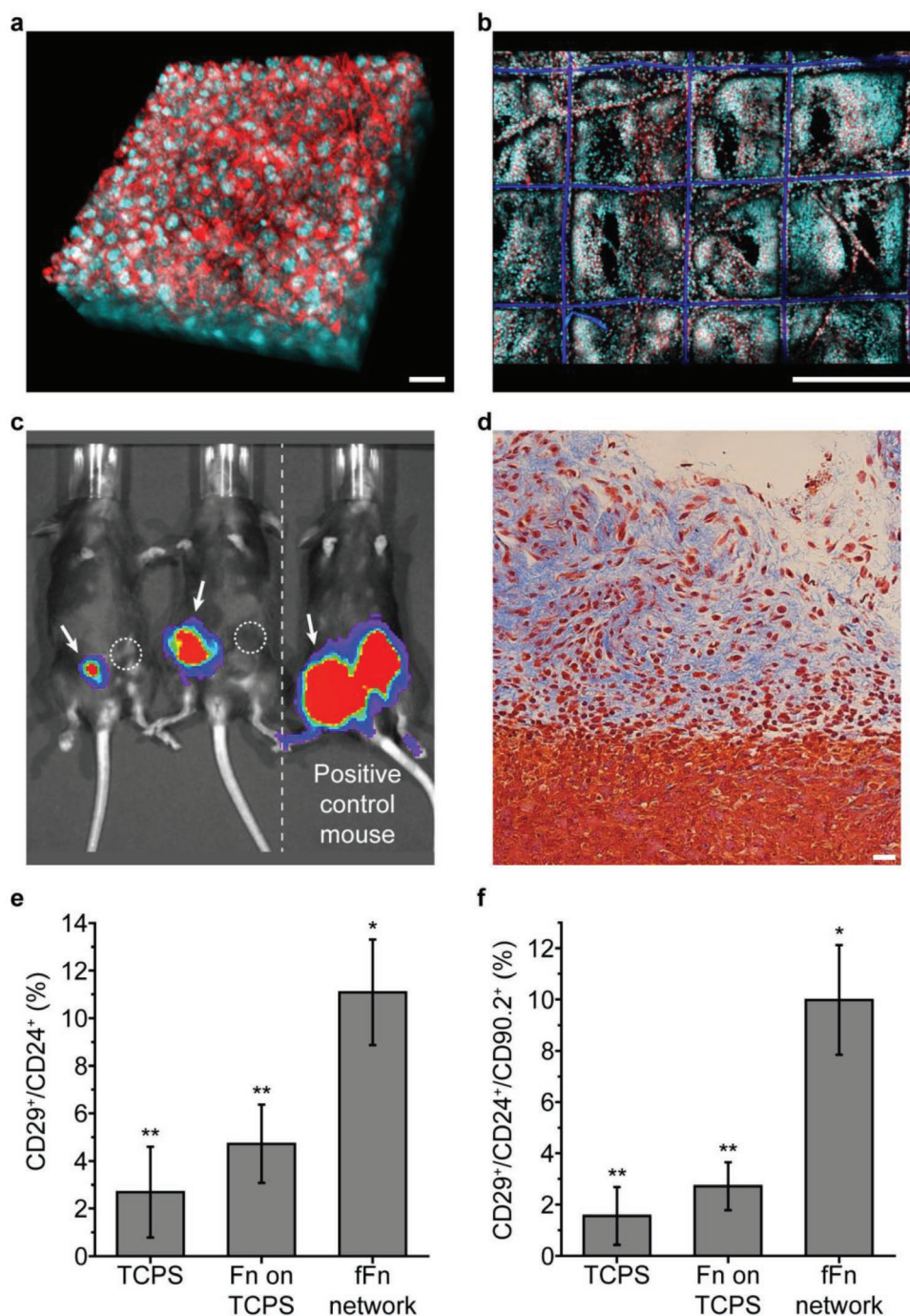


Figure 2. Engineered fFn networks enhance tumor engraftment efficiency in a mouse breast cancer model. a) AT-3 mouse breast cancer cells formed 3D cell volumes approximately 70 μm thick in vitro after three days on fFn networks. Scale bar 25 μm . b) Large-scale view shows that AT-3 cells in (a) proliferated and filled the 3D space within the fFn network. Scale bar 500 μm . a,b) Channels: cyan, cell nucleus; red, actin. c) Bioluminescence image of tumor formation in immune-competent mice 21 d after AT-3 cells were orthotopically implanted (image exposure time 10 s). Mice on the left after implantation of fFn networks carrying about 30 000 AT-3 cells into the mammary fat pads indicated by arrows (group 1). The contralateral mammary fat pad received an injection of approximately the same number of cells suspended in an Fn solution as indicated by circles (group 2). The mouse on the right is a positive control having received the group 3 fFn network in the left mammary fat pad (arrow), and the group 4 injection in the right, each delivering 200 000 AT-3 cells (the minimum required for tumor formation by cell injection^[30]). d) Mason's Trichrome staining of a group 1 tumor graft that formed after 21 d showing AT-3 cells invading the surrounding tissues. Scale bar: 25 μm . e,f) Quantification of the CD29⁺/CD24⁺ population in AT-3 cells capable of self-renewal ($P < 0.05$) (e) and the CD29⁺/CD24⁺/CD90.2⁺ tumor initiating population in AT-3 cells (f). AT-3 cells were cultured three days on TCPS, TCPS with Fn conformally adsorbed (Fn on TCPS), or fFn networks. A single star indicates that the fFn networks are statistically different from TCPS and Fn on TCPS; a double star indicates that TCPS and Fn on TCPS are statistically similar.

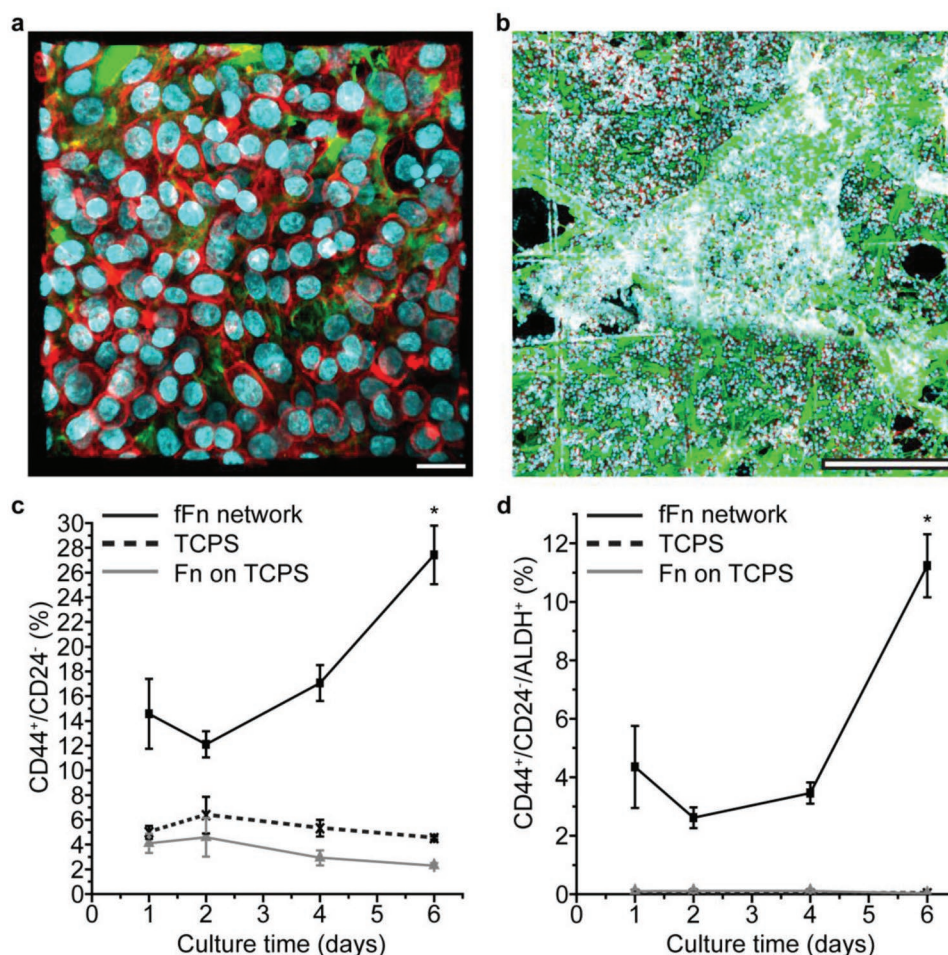


Figure 3. Engineered fFn networks increase the tumor-initiating population in MDA-MB-468 human breast cancer cells. a) MDA-MB-468 breast cancer cells cultured four days on fFn networks form cell–cell and cell–ECM contacts. Scale bar 25 μm . b) MDA-MB-468 cells form large interconnected volumes throughout fFn networks after four days. Scale bar 500 μm . a,b) Channels: green, Fn; orange, laminin; cyan, cell nucleus; and red, actin. c,d) Population of MDA-MB-468s on fFn networks (black solid line and square marker), TCPS (black dotted line and crisscross marker), or Fn adsorbed conformally onto TCPS (gray line and triangular marker) that are CD44⁺/CD24⁻ (c) and CD44⁺/CD24⁻/ALDH⁺ (d) measured at different culture time points. Marker expression for cells on TCPS or Fn on TCPS is significantly lower than that of the fFn network at values nearing zero in d). The starred time point is statistically different from the other three time points within the fFn network data set.

networks showed robust tumor engraftment at cell numbers that were 85% lower than what is typically needed for successful engraftment.^[30] The increased tumorigenicity is consistent with our in vitro findings that AT-3 cells cultured on fFn networks have increased subpopulations of tumor-initiating (CD29⁺/CD24⁺)^[31] and metastatic (CD29⁺/CD24⁺/CD90.2⁺)^[31c,32] cells (Figure 2e,f). We further note that the invasive subpopulation (CD90.2⁺) was nearly 30-fold higher on fFn networks relative to Fn-coated TCPS (Figure S9d, Supporting Information).

We next evaluated if the increased tumorigenicity observed in mouse breast cancer cells would also be observed in human triple negative breast cancer cells. We selected the MDA-MB-468 cell line because less than 3% of the total population express the CD44⁺/CD24⁻ tumor initiating phenotype.^[33] After four days of expansion on fFn networks, MDA-MB-468 cells formed a dense 3D cancer microenvironment over extended areas of about 10 mm² (Figure 3a,b, and Figure S11a, Supporting Information). Compared to cells cultured on either

TCPS or Fn-coated TCPS, the CD44⁺/CD24⁻ subpopulation was significantly higher on fFn networks (Figure 3c). In addition, the CD44⁺/CD24⁻/ALDH⁺ subpopulation significantly increased on fFn networks relative to the control groups for all time points (Figure 3d). CD44⁺/CD24⁻/ALDH⁺ breast cancer cells have higher tumor-initiating potential than either CD44⁺/CD24⁻ or ALDH⁺ populations (ALDH, aldehyde dehydrogenase).^[34] Because the ALDH⁺ subpopulation showed no significant difference relative to the controls after four days in culture on fFn networks (Figure S11b, Supporting Information), the data indicate that enrichment of CD44⁺/CD24⁻/ALDH⁺ cells is largely driven by an increase in the CD44⁺/CD24⁻ subpopulation. These data are consistent with an increased level of EMT in MDA-MB-468 cells after expansion on fFn networks relative to the control groups (Figure 3c, and Figures S11 and S12, Supporting Information).

Stem-like breast cancer cells can secrete extracellular laminin during matrix remodeling to improve self-renewal and

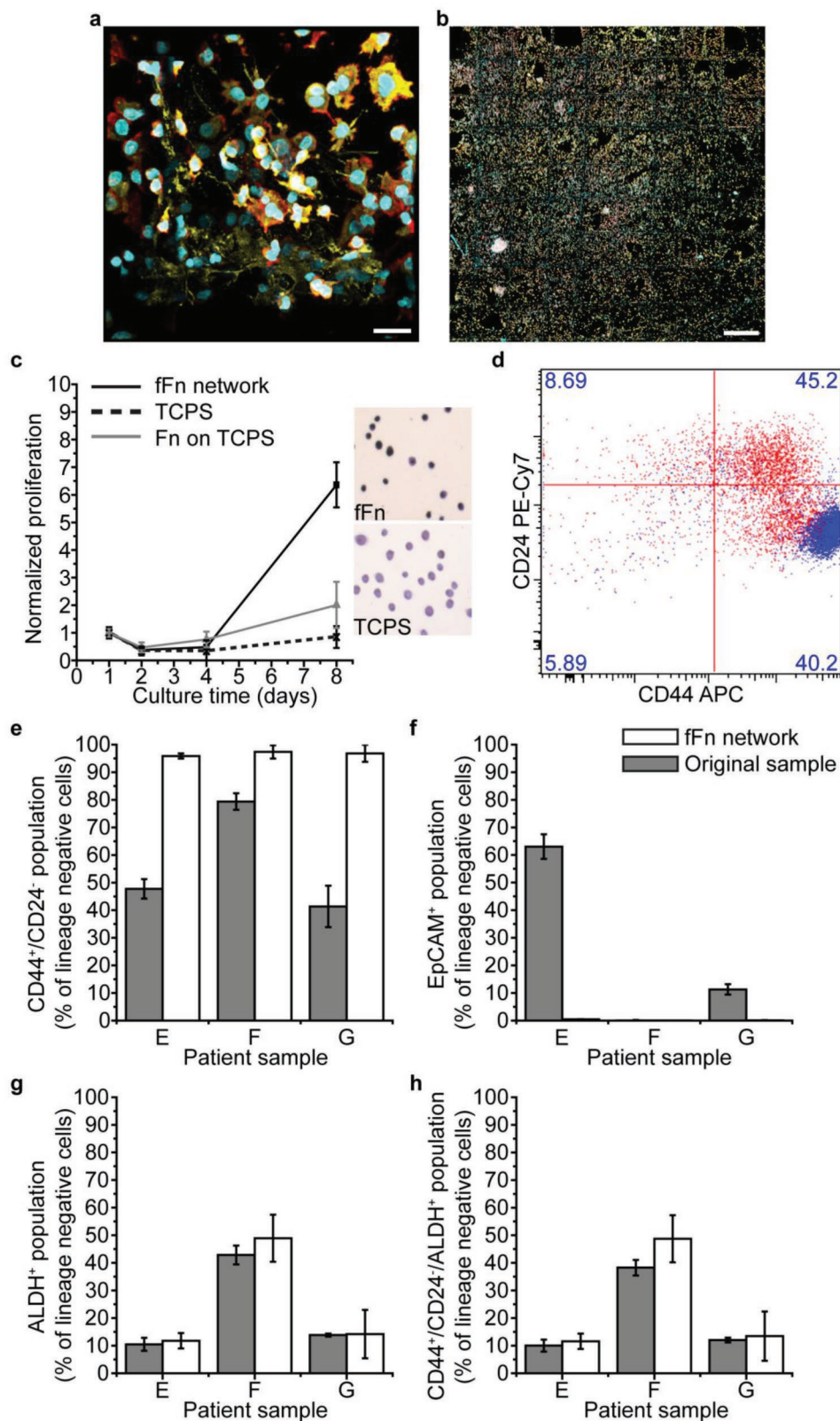


Figure 4. Engineered fFn networks enable expansion of patient breast cancer cells and enrich the tumor-initiating cell population in an EMT. a,b) Four-day culture of heterogenous cell populations from Patient E on fFn networks. Channels: cyan, cell nucleus; red, actin; and yellow, cytokeratin 5. a) 3D cell structures form within the pores and along the microfiber walls of the scaffold. Scale bar 25 μm . b) Patient E cells fill the fFn networks at a large scale across all square 500 μm -wide pores of the tessellated scaffold. Scale bar 500 μm . c) Patient cell proliferation measured via mitochondrial

tumorigenicity.^[35] With the observed enrichment of CD44⁺/CD24⁻ and CD44⁺/CD24⁻/ALDH⁺ in MDA-MB-468 cells after culture on fFn networks, we asked whether significant amounts of endogenous laminin had been incorporated into the ECM, influencing cell phenotype. After four days of MDA-MB-468 cell culture, fFn networks were decellularized^[36] and co-stained for Fn and laminin. MDA-MB-468 cells had only secreted small and sporadic amounts of laminin, while the original fFn network remained intact (Figure S13, Supporting Information). This experiment indicates that Fn is the predominant ECM factor for early EMT transitions on engineered fFn networks.

Facile, reliable expansion of patient-derived breast cancer cells would tremendously advance precision oncology, but still remains an elusive goal.^[37] Mouse tumor xenografts have been used to develop avatars using primary human patient cells, but in breast cancer, this approach suffers from poor cell engraftment and limited cell proliferation.^[37b,38] We therefore evaluated fFn networks as a platform to directly expand patient-derived cells from malignant pleural effusion or ascites samples from 14 women representing a range of ages and molecular subtypes of metastatic breast cancers (Table S1, Supporting Information). We successfully cultured metastatic breast cancer cells on fFn networks from all 14 patient samples. Importantly, cell expansion on fFn networks did not require prior fractionation of the patient samples and resulted in a 36-fold enrichment of the cancer cell population (Figure S14a, Supporting Information). The majority of patients (9 out of 13; one sample was of unknown receptor status) were estrogen receptor positive, a breast cancer subtype that typically is less likely to form tumor grafts.^[33c,37a] Cancer cells from all 14 patient samples proliferated on fFn networks, but not on TCPS or Fn-coated TCPS, as represented in **Figure 4c** and Figure S15b in the Supporting Information. Ki67 staining further indicated that cells were in a proliferative state on fFn networks, but senescent on TCPS^[37a] (Figure 4c). Cells from patient E (patient samples arbitrarily named), which were first cultured on fFn networks for one day, then removed and re-seeded onto TCPS, proliferated for five passages before entering senescence (Figure S15a, Supporting Information). This repeatedly observed finding was in stark contrast to the unsuccessful direct culture of patient cells on TCPS, suggesting the potential use of fFn networks as a preconditioning microenvironment to promote expansion of cancer cells from pleural effusions, an accessible, yet underutilized source of patient tumor cells.

The total patient cell population increased by more than sevenfold relative to the original patient sample over the course of eight days of culture on fFn networks (Figure 4c). In general, diverse cell populations were maintained on fFn networks showing heterogeneity in morphology and expression of cytokeratin 5 (CK5), an epithelial marker (Figure 4a,b and Figure S16a–d, Supporting

Information). After five days of culture, CK5⁺ cells remained in small clusters. By day 10, CK5⁺ cells had expanded and spread out into the open pores of the scaffold (Figure S16d, Supporting Information). Different cell types were often found to spatially segregate as seen in Figure S16a in the Supporting Information, where CK5⁺ cells formed tight clusters on the fFn while actin-rich cells of a spindle-like morphology adhered first to the scaffold microfibers and then proliferated outwards.

Because of their distinct receptor status, patient samples E, F, and G were selected for evaluation of cancer stem cell markers after a six-day culture on fFn networks. Patient breast cancer cells with a mesenchymal CD44⁺/CD24⁻ stem cell phenotype were enriched relative to the percent in the original sample (Figure 4d,e, and Figure S14c, Supporting Information). This finding corroborates earlier results with MDA-MB-468 cells (Figure 3c). The epithelial tumor-initiating subpopulation marked as ALDH⁺ (Figure 4g, and Figure S14b,e, Supporting Information) and the highly tumorigenic overlapping immunotype CD44⁺/CD24⁻/ALDH⁺^[39] (Figure 4h) were maintained on fFn networks compared to the original patient sample (having averages within 10%). Additionally, the percentage of cancer cells expressing the epithelial marker, EpCAM (epithelial cell adhesion molecule), disappeared after culture on fFn networks (Figure 4f, and Figure S14d, Supporting Information). Upregulation of mesenchymal stem-like cancer cells combined with downregulation of EpCAM and maintenance of the ALDH⁺ subpopulation characterizes an EMT, suggesting that fFn networks can induce EMT in breast cancer patient cells cultured in vitro. Despite these observed phenotypic changes, the breast cancer receptor status of the original sample was maintained after the six-day culture on fFn networks (Figure S16e, Supporting Information).

Engineered fFn networks represent a major advance toward the goal of using cancer patient cells to engineer tumor tissue that authentically represents the subtypes, heterogeneity, architecture, and patient-to-patient variability of breast cancer. This work further suggests that Fn may play a role in EMT.^[40] Scaffolds functionalized with our scalable fFn technology produce suitable microenvironments for direct and efficient culture of unfractionated patient samples. In short-term in vitro culture, fFn networks resulted in the expansion of patient samples, where less than 5% of the initial population were cancer cells, to complex cultures or microtumors with cancer cells constituting 36% of the total cell population.

Our results suggest that engineered fFn networks can provide the next-generation 3D cell culture platform for expansion of both immortalized and primary cancer cells in vitro. Harnessing the known ability of Fn to form fibrils under shear

activity is far increased on fFn networks (black solid line and square marker) relative to the little to no growth on Fn adsorbed conformally onto TCPS (gray line and triangular marker), or TCPS alone (black dotted line and crisscross marker). Additionally, the inset shows representative images of Ki67 staining of patient cells cultured on either TCPS or fFn networks. Darker color indicates that the cells are in a proliferative state on fFn networks but senescent on TCPS. d) Flow cytometry measurement of CD24 and CD44 in Patient E cells where the original sample is shown in red and the six day in vitro culture on fFn networks is shown in blue. Cell phenotype concentrated towards CD44⁺/CD24⁻ status after culture on fFn networks. e–h) Flow cytometry measurements of the percentage of lineage negative cells that are CD44⁺/CD24⁻ (e), EpCAM⁺ (epithelial cell adhesion molecule) (f), ALDH⁺ (aldehyde dehydrogenase) (g), and CD44⁺/CD24⁻/ALDH⁺ (h) within samples from patients E, F, and G. Gray bars represent the original patient sample and white bars indicate result after cells were cultured on engineered fFn networks for six days.

forces, we directly suspended fFn across open-pore scaffolds resulting in a platform that is readily implemented in cell culture. These fFn networks allow cells to craft their own micro-environment while we observe the cell response, representing a transformative technology in fundamental cancer studies,^[37b] precision medicine,^[33c] pharmaceutical development,^[37b] and pre-clinical screening.^[37a]

Experimental Section

Scaffold Fabrication: Tessellated scaffolds were made via 3D jet writing as previously described.^[17] Briefly, PLGA was dissolved into a 30 wt% solution of chloroform and N,N-dimethylformamide at a ratio of 93:7. The solution was pumped through a 20 gauge needle at 0.04 mL h⁻¹ with an applied voltage of 16 kV. As the fluid jet descends to the ground electrode, it passes through a copper ring at 9 kV. The jetted fiber is collected on the ground electrode, a stainless-steel plate, which is translated through x-y coordinates by computer-controlled motions to stack the depositing fiber onto itself in a desired pattern. Non-woven mats were made by random deposition of electrospun PLGA fibers onto a flat grounded electrode without use of the copper ring.

Hydrodynamically Induced Fibrillogenesis and Other Fibronectin Substrates: The tessellated scaffold fabricated via 3D jet writing was first secured in a custom-built stainless-steel frame. The framed scaffold was then placed at the center of a 2-mL microcentrifuge tube containing 900 μ L volume of a 111 μ g mL⁻¹ solution of human Fn such that the air, scaffold, and solution formed a three-phase interface when the tube was laid on its side. The tube was placed on a rotisserie rotator at 30 °C and 8 rpm (for an interface velocity of 10.4 mm s⁻¹) for a period of 2 h. The protein-loaded scaffold was then washed three times in Dulbecco's phosphate buffered saline (DPBS) and stored at 4 °C up to one week until use. For suspended collagen networks, 900 μ L of collagen I dissolved in 33 \times 10⁻³ M acetic acid at 2.7 mg mL⁻¹ was combined with 100 μ L of Dulbecco's modified Eagle medium (DMEM) and 140 μ L of 0.34 N NaOH in a 2-mL microcentrifuge tube. The solution turned from yellow to pink with the addition of base. All collagen preparations were performed on ice. The framed scaffold was then secured in the 2-mL tube to form a three-phase interface and rotated for four hours at 27 °C. Conformal Fn coatings onto tessellated scaffolds, smooth TCPS surfaces, or non-woven fiber mats were prepared by statically submerging the substrate in a 111 μ g mL⁻¹ Fn solution for 2 h at 30 °C and overnight at room temperature (RT).

Protein Mass Measurements: A Micro BCA assay (Pierce Biotechnology, Rockford, IL) was used to measure the mass of protein deposited onto the scaffolds. First, the PLGA was degraded in a 0.9 M NaOH solution for 1 h, and then the solution was neutralized in a 0.9 M HCl solution. The mass of protein was determined by measuring the absorption at 562 nm after a 1 h, 60 °C incubation, in the Micro BCA working reagent and referenced to a standard curve of known masses.

ICC Staining: Immunocytochemical (ICC) analysis was performed as previously described.^[17] Briefly, cells on the fFn networks were fixed with a 2% paraformaldehyde overnight. Cells were then permeabilized with a 0.1% Triton X-100 solution for 5 min. The fixed cells were then exposed to a 5% bovine serum albumin (BSA) blocking solution for 1 h before application of the antibodies. Cells were imaged using a Nikon A-1 confocal microscope (Nikon Corp., Minato, Tokyo, Japan). If only protein without cells was present on the fFn network, then Triton X-100 was not used.

SEM Imaging: The tessellated scaffold was sputter coated with gold and visualized with an Amray FE 1900 scanning electron microscope (SEM) with an acceleration voltage of 5 kV. All other SEM images were taken with a Helios 650 Nanolab SEM/FIB by FEI of Thermo Fisher Scientific at voltages ranging from 2 to 5 kV. Prior to SEM, samples of cells or proteins were dehydrated by soaking for 20 min in a series of ethanol solutions increasing in concentration. The

sample was then transferred to a microcentrifuge tube and tertbutanol was added to cover. The tube was placed in liquid nitrogen for two minutes then lyophilized overnight.

Deoxycholate Treatment: fFn networks that were subjected to deoxycholate treatment were submerged in 1% deoxycholate solution overnight on an orbital shaker. fFn networks that were left untreated for comparison to deoxycholate exposure were also rotated overnight in water on the orbital shaker. These fFn networks were prepared using fluorescent Fn that was first conjugated to DyLight-650 using a DyLight antibody labeling kit following manufacturer instructions.

Cell Culture: Malignant pleural effusion and ascites samples from women with metastatic breast cancer were collected with written informed consent from all subjects under a protocol approved by the University of Michigan Institutional Review Board (IRB #2001-0344). These samples were collected for clinical indications, and this research used excess fluid samples that otherwise would be discarded. Total cells were concentrated in samples by centrifugation without additional processing steps prior to seeding onto scaffolds. Breast cancer patient cell samples were seeded in 1 mL onto fFn networks with square scaffold pores 500 μ m wide at a concentration of 2 \times 10⁶ cells mL⁻¹. Cancer cell lines were seeded in 100 μ L at a concentration of 2 \times 10⁶ cells mL⁻¹ for 4 h, then the concentration was diluted to 2 \times 10⁵ cells mL⁻¹. Cells were cultured in DMEM containing 10% fetal bovine serum (FBS), 1% non-essential amino acids (NEAA), 2 \times 10⁻³ M L-glutamine, and 1% antibiotic-antimycotic. Cells were seeded and cultured in low adhesion 24 well plates (Corning Inc., Corning, NY, USA) and maintained at 37 °C in 5% CO₂. Although not always passaged, passaging primary lineage negative cancer cells could be done by placing a cell-free fFn network in contact overnight with another that had already grown confluent with cells.

Proteomics: Lyophilized Fn (Corning) was dissolved in DPBS as described above. The protein concentration was determined by Qubit fluorometry (Invitrogen). 10 μ g of the sample was processed by sodium dodecyl sulfate-polyacrylamide gel electrophoresis (SDS-PAGE) using a 10% Bis-Tris NuPage mini-gel with the 3-(N-morpholino)propanesulfonic acid (MOPS) buffer system. The mobility region was excised and processed by in-gel digestion using a robot (ProGest, DigiLab) using the following procedure: washed with 25 \times 10⁻³ M ammonium bicarbonate followed by acetonitrile, reduced with 10 \times 10⁻³ M dithiothreitol at 60 °C followed by alkylation with 50 \times 10⁻³ M iodoacetamide at RT, digested with sequencing grade trypsin (Promega) at 37 °C for 4h, and quenched with formic acid. Then the supernatant was analyzed directly without further processing. Half of the gel digest was analyzed by nano LC-MS/MS with a Waters NanoAcquity HPLC system interfaced to a ThermoFisher Q Exactive. Peptides were loaded on a trapping column and eluted over a 75 μ m analytical column at 350 nL min⁻¹; both columns were packed with Luna C18 resin (Phenomenex). The mass spectrometer was operated in data-dependent mode, with the Orbitrap operating at 70 000 and 17 500 FWHM for MS and MS/MS respectively. The fifteen most abundant ions were selected for MS/MS. Data were searched using a local copy of Mascot (Matrix Science) with the following parameters: Enzyme:Trypsin/P; Database:SwissProt Human (concatenated forward and reverse plus common contaminants); Fixed modification: Carbamidomethyl (C); Variable modifications: none; mass values: monoisotopic; peptide mass tolerance: 10 ppm; fragment mass tolerance: 0.02 Da; maximum missed cleavages: 2. Mascot dat-files were parsed into Scaffold (Proteome Software) for validation, filtering and to create a non-redundant protein list. Data were filtered using a threshold for the false discovery rate (FDR) of 1% protein and requiring at least two unique peptides per protein.

Proliferation Assays: AT-3 mouse breast cancer cells and human breast cancer cell lines T47D and SUM159 all stably expressed firefly luciferase. Proliferation was tracked over time by administering 15 mg mL⁻¹ D-luciferin to the cell medium at a ratio of 1:100 and incubating for 10 min before the relative light intensity was measured using a luminometer (Perkin Elmer MLD2300-000). The growth rates of the primary patient samples and the MDA-MB-468 cell line were evaluated by measuring changes in mitochondrial activity using a resazurin-based assay kit (Tox-8,

Sigma–Aldrich, St. Louis, MO, USA) following the manufacturer guidelines. The initial signal was recorded after seeding, and then subsequent mitochondrial activity measurements were normalized to the initial time point. Additionally, Ki67 staining was used to determine whether the primary patient samples were in a proliferative or senescent state.

Decellularization: If cells were removed from fFn networks to visualize the remaining protein matrix, samples were decellularized in a protocol adapted from Lu et al.^[36] Samples were washed with phosphate buffered saline (PBS), then deionized (DI) water, and immersed in a solution of 0.1% Triton X-100 with 1.5 M KCl in 50×10^{-3} M Tris buffer on a slow-moving shaker for two hours at 4 °C. Samples were washed in 10×10^{-3} M Tris buffer, followed by DI water for one hour each. The remaining protein matrix was fixed and stained via ICC protocol.

Animal Protocol: All animal studies were approved by the University of Michigan Institutional Animal Care and Use Committee. Briefly, 6–8-week-old female C57BL/6 mice (Charles River Laboratories Inc., Wilmington, MA, USA) were anesthetized using 1–2% isoflurane at a flowing oxygen rate of 1 L min⁻¹ (EZ150 Isoflurane Vaporizer, EZ Anesthesia), and an incision was made to expose the mammary fat pad. A fFn network carrying AT-3 cells was then placed directly into the fat pad^[30] and the incision was closed with wound clips. The number of AT-3 cells on the scaffold was verified using luminescence. 15 mg mL⁻¹ D-luciferin was added to the cell medium at a ratio of 1:100 and incubated for 10 min before the relative light intensity was measured using a luminometer (Perkin Elmer MLD2300-000) and compared with a standard curve. Tumor engraftment was evaluated using bioluminescence imaging.^[30]

Flow Cytometry: Cells were stained following a previously established protocol.^[39,41] Cells were removed using 0.25% trypsin, which was neutralized using a 3:1 volume of complete medium. Cells were then counted using a Luna-FL dual fluorescence cell counter (Logos Biosystems, Dongan-gu, Anyang-si, Gyeonggi-do, South Korea), and re-suspended in aldefluor buffer. Antibodies were added and incubated for 30 min, and then rinsed with aldefluor buffer. For primary patient sample analysis, the cells were first incubated in the lineage cocktail for 30 min, before staining for EpCAM, CD44, CD24, and ALDH activity. MDA-MB-468 cells were used to establish single color channels. Isotype controls were used to establish gating for the CD44, EpCAM, lineage negative cells, and CD24.^[39,41] N,N-diethylaminobenzaldehyde (DEAB) was used to establish gating for the aldefluor activity assay.^[39]

Histology: Tumor histology was evaluated by first fixing with 4% formalin for 24 h. Then, the tissue was prepared for histology by dehydrating in ethanol, sealed with paraffin, and sliced for staining with Masson's trichrome.

Statistics: Statistical analysis was performed using Minitab (Minitab Inc., State College, PA, USA). One-way analysis of variance (ANOVA, $p < 0.05$) was used to determine statistical significance. Tukey multicomparison testing was performed to determine differences between groups. All data were reported as the mean \pm standard deviation.

Supporting Information

Supporting Information is available from the Wiley Online Library or from the author.

Acknowledgements

The authors acknowledge funding under U01CA210152 from the National Cancer Institute. The authors also thank the UM Center for Molecular Imaging for bioluminescence imaging instrumentation, the UM Microscopy and Imaging Laboratory for laser scanning confocal microscopy (LSCM) access, the Michigan Center for Materials Characterization for SEM access, Henriette A. Remmer and the University of Michigan Medical School Proteomics and Peptide

Synthesis Core for FFn sequencing, funding from FFANY Shoes on Sale, and the lab of Diane M. Simeone for pancreatic cancer cells. S.J. acknowledges support from the National Science Foundation Graduate Research Fellowship Program: DGE 1256260. L.S. acknowledges support from the Department of Defense Breast Cancer Research Post-Doctoral Fellowship: W81XWH-10-1-0582. D.B.N. acknowledges NIH support from the Biotechnology Predoctoral Research Training Program, grant T32 GM008353. J.H.J. acknowledges the support of NIH's Microfluidics in Biomedical Sciences Training Program: NIH NIBIB T32 EB005582. G.D.L. acknowledges NIH grants R01CA196018. Finally, the authors are thankful to Ayse Muniz and Dr. Tae-Hwa Chun, University of Michigan, for enlightening discussions.

Conflict of Interest

The authors declare no conflict of interest.

Keywords

3D cell culture, extracellular matrix, fibrillar fibronectin, protein–polymer composites, tumor microenvironment

Received: July 17, 2019

Published online: September 30, 2019

- [1] M. Cantini, P. Rico, M. Salmeron-Sanchez, in *Biomimetic Approaches for Biomaterials Development* (Ed: J. F. Mano), Wiley-VCH, Weinheim, Germany **2012**, p. 189.
- [2] J. Lee, M. J. Cuddihy, N. A. Kotov, *Tissue Eng., Part B* **2008**, *14*, 61.
- [3] T. Boonthekul, D. J. Mooney, *Curr. Opin. Biotechnol.* **2003**, *14*, 559.
- [4] J. Ulmer, B. Geiger, J. P. Spatz, *Soft Matter* **2008**, *4*, 1998.
- [5] J. P. Wang, A. Hielscher, *J. Cancer* **2017**, *8*, 674.
- [6] J. L. Leight, M. A. Wozniak, S. Chen, M. L. Lynch, C. S. Chen, *Mol. Biol. Cell* **2012**, *23*, 781.
- [7] R. N. Kaplan, R. D. Riba, S. Zacharoulis, A. H. Bramley, L. Vincent, C. Costa, D. D. MacDonald, D. K. Jin, K. Shido, S. A. Kerns, Z. Zhu, *Nature* **2005**, *438*, 820.
- [8] a) M. Mitsi, S. Handschin, I. Gerber, R. Schwartlander, E. Klotzsch, R. Wepf, V. Vogel, *Biomaterials* **2015**, *36*, 66; b) W. S. To, K. S. Midwood, *Fibrog. Tissue Repair* **2011**, *4*, 21; c) K. Wang, R. C. Andresen Eguiluz, F. Wu, B. R. Seo, C. Fischbach, D. Gourdon, *Biomaterials* **2015**, *54*, 63.
- [9] a) K. Wang, B. R. Seo, C. Fischbach, D. Gourdon, *Cell Mol. Bioeng.* **2016**, *9*, 1; b) P. Singh, C. Carraher, J. E. Schwarzbauer, *Annu. Rev. Cell Dev. Biol.* **2010**, *26*, 397.
- [10] a) B. Cseh, S. Fernandez-Sauze, D. Grall, S. Schaub, E. Doma, E. Van Obberghen-Schilling, *J. Cell Sci.* **2010**, *123*, 3989; b) I. Wierzbicka-Patynowski, J. E. Schwarzbauer, *J. Cell Sci.* **2003**, *116*, 3269; c) G. Baneyx, L. Baugh, V. Vogel, *Proc. Natl. Acad. Sci. USA* **2002**, *99*, 5139.
- [11] C. A. Lemmon, S. H. Weinberg, *Sci. Rep.* **2017**, *7*, 18061.
- [12] W. C. Little, M. L. Smith, V. Vogel, *Matrix Biol.* **2008**, *27*, 451.
- [13] a) O. S. Ejim, G. W. Blunn, R. A. Brown, *Biomaterials* **1993**, *14*, 743; b) R. A. Brown, G. W. Blunn, O. S. Ejim, *Biomaterials* **1994**, *15*, 457.
- [14] S. Ahn, L. F. Deravi, S. Park, B. E. Dabiri, J. Kim, K. K. Parker, K. Shin, *Adv. Mater.* **2015**, *27*, 2838.
- [15] N. Pernodet, M. Rafailovich, J. Sokolov, D. Xu, N. L. Yang, K. McLeod, *J. Biomed. Mater. Res.* **2003**, *64A*, 684.
- [16] L. F. Deravi, T. Su, J. A. Paten, J. W. Ruberti, K. Bertoldi, K. K. Parker, *Nano Lett.* **2012**, *12*, 5587.

- [17] J. H. Jordahl, L. Solorio, H. Sun, S. Ramcharan, C. B. Teeple, H. R. Haley, K. J. Lee, T. W. Eyster, G. D. Luker, P. H. Krebsbach, J. Lahann, *Adv. Mater.* **2018**, *30*, 1707196.
- [18] a) F. J. Fogerty, S. K. Akiyama, K. M. Yamada, D. F. Mosher, *J. Cell Biol.* **1990**, *111*, 699; b) H. Bultmann, A. J. Santas, D. M. Peters, *J. Biol. Chem.* **1998**, *273*, 2601; c) P. J. McKeown-Longo, D. F. Mosher, *J. Cell Biol.* **1983**, *97*, 466.
- [19] a) Y. F. Liao, K. G. Wieder, J. M. Classen, L. Van De Water, *J. Biol. Chem.* **1999**, *274*, 17876; b) L. Borsi, B. Carnemolla, P. Castellani, C. Rosellini, D. Vecchio, G. Allemanni, S. E. Chang, J. Taylor-Papadimitriou, H. Pande, L. Zardi, *J. Cell Biol.* **1987**, *104*, 595.
- [20] a) S. D. Kanters, J. D. Banga, A. Algra, R. C. Frijns, J. J. Beutler, R. Fijnheer, *Diabetes Care* **2001**, *24*, 323; b) M. Castellanos, R. Leira, J. Serena, M. Blanco, S. Pedraza, J. Castillo, A. Davalos, *Stroke* **2004**, *35*, 1671.
- [21] M. Leiss, K. Beckmann, A. Giros, M. Costell, R. Fassler, *Curr. Opin. Cell Biol.* **2008**, *20*, 502.
- [22] Y. Abe, N. A. Bui-Thanh, C. M. Ballantyne, A. R. Burns, *Biochem. Biophys. Res. Commun.* **2005**, *338*, 1640.
- [23] R. Manabe, N. Ohe, T. Maeda, T. Fukuda, K. Sekiguchi, *J. Cell Biol.* **1997**, *139*, 295.
- [24] D. Missirlis, T. Haraszti, H. Kessler, J. P. Spatz, *Sci. Rep.* **2017**, *7*, 3711.
- [25] A. J. Zollinger, M. L. Smith, *Matrix Biol.* **2017**, *60–61*, 27.
- [26] Y. Mao, J. E. Schwarzbauer, *Matrix Biol.* **2005**, *24*, 389.
- [27] E. Klotzsch, M. L. Smith, K. E. Kubow, S. Muntwyler, W. C. Little, F. Beyeler, D. Gourdon, B. J. Nelson, V. Vogel, *Proc. Natl. Acad. Sci. USA* **2009**, *106*, 18267.
- [28] M. L. Smith, D. Gourdon, W. C. Little, K. E. Kubow, R. A. Eguiluz, S. Luna-Morris, V. Vogel, *PLoS Biol.* **2007**, *5*, e268.
- [29] B. Fernandez-Garcia, N. Eiro, L. Marin, S. Gonzalez-Reyes, L. O. Gonzalez, M. L. Lamelas, F. J. Vizoso, *Histopathology* **2014**, *64*, 512.
- [30] J. Fenner, A. C. Stacer, F. Winterroth, T. D. Johnson, K. E. Luker, G. D. Luker, *Sci. Rep.* **2015**, *4*, 5512.
- [31] a) R. W. Cho, X. Wang, M. Deihn, K. Shedden, G. Y. Chen, G. Sherlock, A. Gurney, J. Lewicki, M. F. Clarke, *Stem Cells* **2008**, *26*, 364; b) I. Malanchi, A. Santamaria-Martinez, E. Susanto, H. Peng, H. Lehr, J. Delaloye, J. Huelsken, *Nature* **2012**, *481*, 85; c) M. Zhang, F. Behbod, R. L. Atkinson, M. D. Landis, F. Kittrell, D. Edwards, D. Medina, A. Tsimelzon, S. Hilsenbeck, J. E. Green, A. M. Michalowska, J. M. Rosen, *Cancer Res.* **2008**, *68*, 4674.
- [32] A. R. Lobba, M. F. Forni, A. C. Carreira, M. C. Sogayar, *Cytometry Part A.* **2012**, *81A*, 1084.
- [33] a) A. K. Croker, D. Goodale, J. Chu, C. Postenka, B. D. Hedley, D. A. Hess, A. L. Allan, *J. Cell. Mol. Med.* **2009**, *13*, 2236; b) C. Sheridan, H. Kishimoto, R. K. Fuchs, S. Mehrotra, P. BhatNakshatri, C. H. Turner, R. Goulet Jr., S. Badve, H. Nakshatri, *Breast Cancer Res.* **2006**, *8*, R59; c) P. Kabos, J. Finlay-Schultz, C. Li, E. Kline, C. Finlayson, J. Wisell, C. A. Manuel, S. M. Edgerton, J. C. Harrell, A. Elias, C. A. Sartorius, *Breast Cancer Res. Treat.* **2012**, *135*, 415.
- [34] a) T. Tanei, K. Morimoto, K. Shimazu, S. J. Kim, Y. Tanji, T. Taguchi, Y. Tamaki, S. Noguchi, *Clin. Cancer Res.* **2009**, *15*, 4234; b) E. Charafe-Jauffret, C. Ginestier, F. Iovino, J. Wicinski, N. Cervera, P. Finetti, M. Hur, M. E. Diebel, F. Monville, J. Dutcher, M. Brown, P. Viens, L. Xerri, F. Bertucci, G. Stassi, G. Dontu, D. Birnbaum, M. S. Wicha, *Cancer Res.* **2009**, *69*, 1302.
- [35] C. Chang, H. L. Goel, H. Gao, B. M. Pursell, L. D. Shultz, D. L. Greiner, S. Ingerpuu, M. Patarroyo, S. Cao, E. Lim, J. Mao, K. K. McKee, P. D. Yurchenco, A. M. Mercurio, *Genes Dev.* **2015**, *29*, 1.
- [36] H. Lu, T. Hoshiba, N. Kawazoe, G. Chen, *J. Biomed. Mater. Res. A.* **2012**, *100*, 2507.
- [37] a) E. Marangoni, A. Vincent-Salomon, N. Auger, A. Degeorges, F. Assayag, P. de Cremoux, L. de Plater, C. Guyader, G. De Pinieux, J. Judde, M. Rebutti, C. Tran-Perennou, X. Sastre-Garau, B. Sigal-Zafrani, O. Delattre, V. Dieras, M. Poupon, *Clin. Cancer Res.* **2007**, *13*, 3989; b) Y. S. DeRose, G. Wang, Y. Lin, P. S. Bernard, S. S. Buys, M. T. W. Ebbert, R. Factor, C. Matsen, B. A. Milash, E. Nelson, L. Neumayer, R. L. Randall, I. J. Stijleman, B. E. Welm, A. L. Welm, *Nat. Med.* **2011**, *17*, 1514.
- [38] X. Zhang, S. Claerhout, A. Prat, L. E. Dobrolecki, I. Petrovic, Q. Lai, M. D. Landis, L. Wiechmann, R. Schiff, M. Giuliano, H. Wong, S. W. Fuqua, A. Contreras, C. Gutierrez, J. Huang, S. Mao, A. C. Pavlick, A. M. Froehlich, M. Wu, A. Tsimelzon, S. G. Hilsenbeck, E. S. Chen, P. Zuloaga, C. A. Shaw, M. F. Rimawi, C. Perou, G. B. Mills, J. C. Chang, M. T. Lewis, *Cancer Res.* **2013**, *73*, 4885.
- [39] C. Ginestier, M. H. Hur, E. Charafe-Jauffret, F. Monville, J. Dutcher, M. Brown, J. Jacquemier, P. Viens, C. G. Kleer, S. Liu, A. Schott, D. Hayes, D. Birnbaum, M. S. Wicha, G. Dontu, *Cell Stem Cell* **2007**, *1*, 555.
- [40] S. A. Mani, W. Guo, M. J. Liao, E. N. Eaton, A. Ayyanan, A. Y. Zhou, M. Brooks, F. Reinhard, C. C. Zhang, M. Shipitsin, L. L. Campbell, K. Polyak, C. Brisken, J. Yang, R. A. Weinberg, *Cell* **2008**, *133*, 704.
- [41] M. Al-Hajj, M. S. Wicha, A. Benito-Hernandez, S. J. Morrison, M. F. Clarke, *Proc. Natl. Acad. Sci. USA* **2003**, *100*, 3983.